Journal of Inorganic and General Chemistry
ZAAC
Zeitschrift für anorganische und allgemeine Chemie
www.zaac.wiley-vch.de
RESEARCH ARTICLE
Check for updates
DOI: 10.1002/zaac.202200384

Special Collection

Understanding the enhanced reactivity of strained intramolecular Frustrated Lewis Pairs

Susana Portela[a] and Israel Fernández*[a]

The poorly understood factors controlling the enhanced reactivity of strained intramolecular frustrated Lewis pairs (FLPs) having a rigid biphenylene tether have been quantitatively explored in detail by means of computational methods. With the help of the activation strain model of reactivity and the energy decomposition analysis methods, the challenging allene activation reaction has been selected and compared to the analogous process mediated by a related intramolecular FLP having a more flexible tether, which is significantly less reactive. In addition, the influence of the nature of the Lewis acid atom on the reactivity of the strained FLP has been considered as well showing that the reactivity steadily decreases when going down in group 13.

Introduction

Since the groundbreaking report by Stephan and co-workers on the metal-free and reversible activation of H_2 by $(C_6H_2Me_3)_2P{-}(C_6F_4){-}B(C_6F_5)_2$,[1] the chemistry of frustrated Lewis Pairs (FLPs) has experienced a tremendous development.[2,3] These species, typically composed of a pair of sterically encumbered Lewis acid (LA) and Lewis base (LB) where the formation of a classical donor–acceptor bond is hampered, exhibit a rich and unique reactivity as a consequence of the cooperative action of their FLP antagonists. For instance, FLPs have been used for not only the activation of dihydrogen but also other small molecules (such as CO, CO_2, N_2O, SO_2, etc.)[2,3] and also promote other interesting processes spanning from hydrogenations of unsaturated compounds[4] to polymerization reactions[5] or heterogeneous catalysis.[6]

Due to the usefulness of FLPs, much progress has been made to produce more active systems, particularly in recent years. For instance, intramolecular FLPs[7] or systems having transition-metal fragments in their structures[8] should be particularly highlighted. In this regard, Limberg and co-workers very recently prepared the highly active intramolecular P/Al FLP **1** having a rigid biphenylene tether, which is able to not only activate CO_2 at room temperature but also, for the first time in the chemistry of FLP, a molecule of allene (Scheme 1).[9]

Although the enhanced reactivity of this FLP was mainly attributed to the release of the strain in the initial FLP upon binding to CO_2 or allene, the ultimate factors controlling the reactivity of this system are not fully understood so far. For this reason, herein we decided to explore the reactivity of this strained FLP toward allene in detail by applying the Activation Strain Model (ASM)[10] of reactivity in combination with the Energy Decomposition Analysis (EDA)[11] method. This ASM-EDA approach was selected because it has greatly contributed to our current understanding of fundamental transformations in chemistry,[12] and particularly, to the chemistry of FLPs.[13,14] We shall first compare the reactivity of **1** with the analogous intramolecular unstrained system **2** having a much more flexible tether connecting the LB and LA centers (Scheme 2). In addition, the influence of the nature of the LA atom on the reactivity of the system shall be investigated as well.

Computational Details

Geometry optimizations of the molecules were performed without symmetry constraints using the Gaussian09 (RevD.01) suite of programs[15] at the dispersion-corrected B3LYP[16]-D3[17]/def2-SVP[18] level including solvent effects (solvent = benzene) with the Polarization Continuum Model (PCM) method.[19] Reactants and adducts were characterized by frequency calculations and have positive definite Hessian matrices. Transition states show only one negative

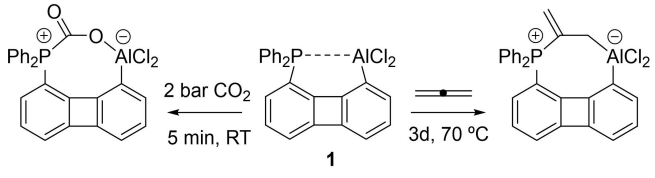

Scheme 1. Reactivity of strained intramolecular FLP **1** reported by Limberg and co-workers (see ref. [9]).

[a] S. Portela, Prof. Dr. I. Fernández
Departmento de Química Orgánica and Centro de Innovación en Química Avanzada (ORFEO-CINQA)
Facultad de Ciencias Químicas, Universidad Complutense de Madrid
Ciudad Universitaria, 28040 Madrid, Spain
E-mail: israel@quim.ucm.es

Supporting information for this article is available on the WWW under https://doi.org/10.1002/zaac.202200384

Special Collection *This article is part of a Special Collection dedicated to Professor Doug Stephan on the occasion of his 70th birthday. Please see our homepage for more articles in the collection.*

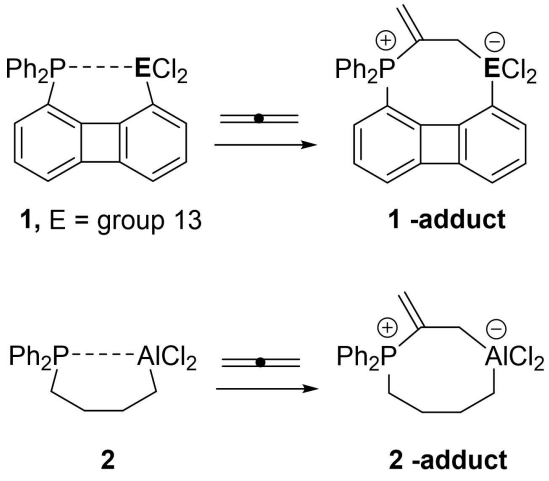

Scheme 2. Reactions involving FLPs **1** and **2** considered in this study.

eigenvalue in their diagonalized force constant matrices, and their associated eigenvectors were confirmed to correspond to the motion along the reaction coordinate under consideration using the Intrinsic Reaction Coordinate (IRC) method.[20] Energy refinements were carried out by means of single-point calculations at the accurate M06-2X[21] level using the much larger triple-ζ basis set def2-TZVPP.[18] This level is denoted PCM(benzene)-M06-2X/def2-TZVPP//PCM(benzene)-B3LYP-D3/def2-SVP. In all cases, the default integration grid was used. Nevertheless, we found that higher integration grids (ultrafine/superfine) lead to nearly identical relative energies (see Figure S1 in the Supporting Information).

Activation Strain Model (ASM) of Reactivity and Energy Decomposition Analysis (EDA) Methods

Within the ASM method,[10] also known as the distortion/interaction model,[10c] the potential energy surface $\Delta E(\zeta)$ is decomposed along the reaction coordinate, ζ, into two contributions, namely the strain $\Delta E_{strain}(\zeta)$ associated with the deformation (or distortion) required by the individual reactants during the process and the interaction $\Delta E_{int}(\zeta)$ between these increasingly deformed reactants:

$$\Delta E(\zeta) = \Delta E_{strain}(\zeta) + \Delta E_{int}(\zeta)$$

Within the EDA method,[11] the interaction energy can be further decomposed into the following chemically meaningful terms:

$$\Delta E_{int}(\zeta) = \Delta V_{elstat}(\zeta) + \Delta E_{Pauli}(\zeta) + \Delta E_{orb}(\zeta) + \Delta E_{disp}(\zeta)$$

The term ΔV_{elstat} corresponds to the classical electrostatic interaction between the unperturbed charge distributions of the deformed reactants and is usually attractive. The Pauli repulsion ΔE_{Pauli} comprises the destabilizing interactions between occupied orbitals and is responsible for any steric repulsion. The orbital interaction ΔE_{orb} accounts for bond pair formation, charge transfer (interaction between occupied orbitals on one moiety with unoccupied orbitals on the other, including HOMO-LUMO interactions), and polarization (empty-occupied orbital mixing on one fragment due to the presence of another fragment). Finally, the ΔE_{disp} term accounts for the interactions coming from dispersion forces. Moreover, the NOCV (Natural Orbital for Chemical Valence)[22] extension of the EDA method has been also used to further partition the ΔE_{orb} term. The EDA-NOCV approach provides pairwise energy contributions for each pair of interacting orbitals to the total bond energy.

The program package ADF[23] was used for EDA calculations using the optimized PCM(benzene)-B3LYP-D3/def2-SVP geometries at the same B3LYP-D3 level in conjunction with a triple-ζ-quality basis set using uncontracted Slater-type orbitals (STOs) augmented by two sets of polarization functions with a frozen-core approximation for the core electrons.[24] Auxiliary sets of s, p, d, f, and g STOs were used to fit the molecular densities and to represent the Coulomb and exchange potentials accurately in each SCF cycle.[25] Scalar relativistic effects were incorporated by applying the zeroth-order regular approximation (ZORA).[26] This level of theory is denoted ZORA-B3LYP-D3/TZ2P//PCM(benzene)-B3LYP-D3/def2-SVP.

Results and Discussion

We first compared the activation of allene by FLPs **1-Al** and **2-Al** to understand the role of the strained nature of the tether connecting the LA and LB on the reactivity. As depicted in Figure 1, both processes exhibit rather similar reaction profiles in the sense that the allene activation takes place in a concerted manner through an eight-membered ring transition state (**TS**) which affords the corresponding zwitterionic adduct in an exergonic transformation. Despite that, from the data in Figure 1, it becomes evident that the presence of the rigid biphenylene linker in the FLP makes compound **1-Al** much more reactive than **2-Al** (having a much more flexible tether) from both kinetic ($\Delta\Delta G^{\neq} \approx 13$ kcal mol^{-1}) and thermodynamic

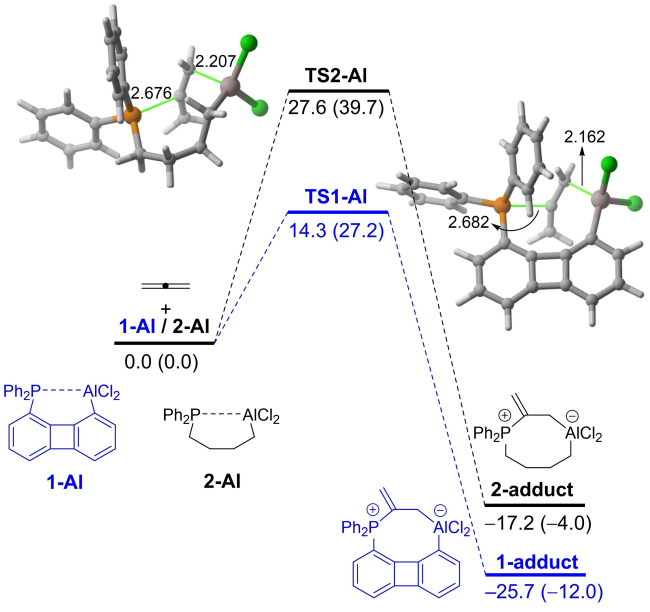

Figure 1. Computed reaction profiles for the allene activations promoted by FLPs **1-Al** and **2-Al**. Relative electronic (ΔE) and free (ΔG, within parentheses) energies and bond distances are given in kcal/mol and angstroms, respectively. All data have been computed at the PCM(benzene)-M06-2X/def2-TZVPP//PCM(benzene)-B3LYP-D3/def2-SVP level.

($\Delta\Delta G_R = 8$ kcal mol^{-1}) points of view. Moreover, the computed barrier for the process mediated by **1-Al** is compatible with the reaction conditions used experimentally (70 °C),[9] which provides support to the selected computational method.

To quantitatively understand the reasons behind the enhanced reactivity of the strained FLP **1-Al**, the Activation Strain Model (ASM) of reactivity was applied next. Figure 2 shows the computed activation strain diagrams (ASDs) for the allene activation reactions promoted by **1-Al** and **2-Al** from the initial stages of the transformations to the respective transition states and projected onto the P···C bond-forming distance. From the data in Figure 2, the **1-Al**-mediated reaction clearly benefits from a less destabilizing strain energy (measured by the ΔE_{strain} term) along the entire reaction coordinate. Our calculations indicate that whereas the energy penalty to deform the allene reactant is rather similar in both activation processes, the deformation energy of the FLP reactant is substantially higher for **2-Al** than for its strained counterpart **1-Al** (see Figure S2 in the Supporting Information) This indicates that the initial geometry of **1-Al**, imposed by the rigid biphenylene tether, better fits into the geometry adopted in the corresponding transition state as compared to **2-Al**. Interestingly, the process mediated by **1-Al** also benefits from a stronger interaction between the deformed reactants, again along the entire reaction coordinate. Therefore, it can be concluded that the lower barrier computed for the allene activation reaction promoted by the strained FLP **1-Al** finds its origin not only in the much lower deformation energy required to adopt the geometry of the corresponding transition state but also in the stronger interaction between the deformed reactants (measured by the ΔE_{int} term). This finding resembles that in strained cycloalkynes in Diels-Alder cycloaddition reactions, where predistorsion not only leads to a reduced strain energy but also enhances the interaction energy between the deformed reactants.[27]

The Energy Decomposition Analysis (EDA) method was applied next to quantitatively understand the factors leading to the stronger interaction energy computed for the reaction involving **1-Al** + allene. Figure 3 graphically shows the evolution of the EDA contributors along the reaction coordinate for both activation reactions once again from the initial stages of the transformation to the respective transition states and projected onto the P···C bond-forming distance. Data in Figure 3 indicate that at the transition state region (i.e. where the barrier takes place), the stronger interaction between the deformed reactants computed for the process involving **1-Al** derives almost exclusively from stronger orbital interactions (measured by the ΔE_{orb} term) and, to a much lesser extent, to a less destabilizing Pauli repulsion (ΔE_{Pauli}). For instance, at the same consistent P···C bond forming distance of 2.7 Å,[28] the difference in the total interaction energy, $\Delta\Delta E_{int} = 3.9$ kcal/mol, roughly matches that of the orbital interactions, $\Delta\Delta E_{orb} = 3.5$ kcal/mol, while the difference in the other attractive terms can be considered as negligible ($\Delta\Delta V_{elstat} = 0.7$ kcal/mol and $\Delta\Delta E_{disp} = 0.1$ kcal/mol).

Furthermore, by means of the Natural Orbitals for Chemical Valence (NOCV) extension of the EDA method, we can not only visualize but also quantify the main pairwise orbital interactions responsible for the stronger ΔE_{orb} computed for the process involving the strained FLP **1-Al**. This method identifies two main orbital interactions dominating the total ΔE_{orb} term, namely the electronic donation from the Lewis base (lone-pair of the phosphorous atom) to the π*(C=C) molecular orbital of the allene (LP(P)→π*(allene), denoted as ϱ_1) and the donation from the occupied π(C=C) of the allene to the Lewis acid (vacant p_z atomic orbital of the aluminum atom), i.e. π(C=C)→p(Al), (denoted as ϱ_2, see Figure 4). The above results clearly

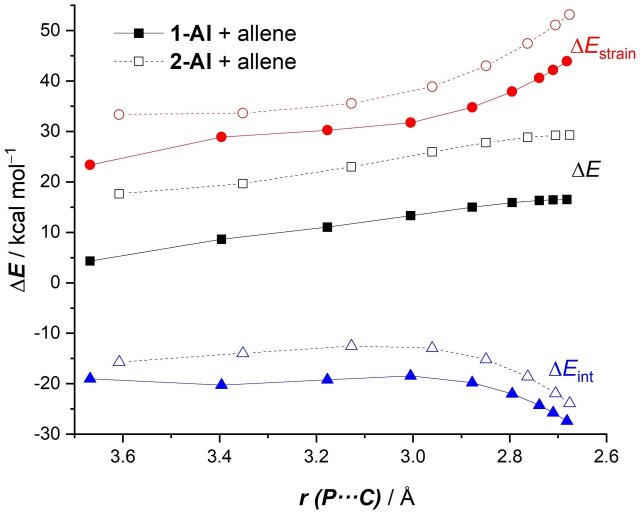

Figure 2. Comparative activation strain analyses of the allene activation reactions mediated by **1-Al** (solid lines) and **2-Al** (dashes lines) projected onto the P···C bond-forming distance. All data have been computed at the PCM(benzene)-B3LYP-D3/def2-TZVPP//PCM(benzene)-B3LYP-D3/def2-SVP level.

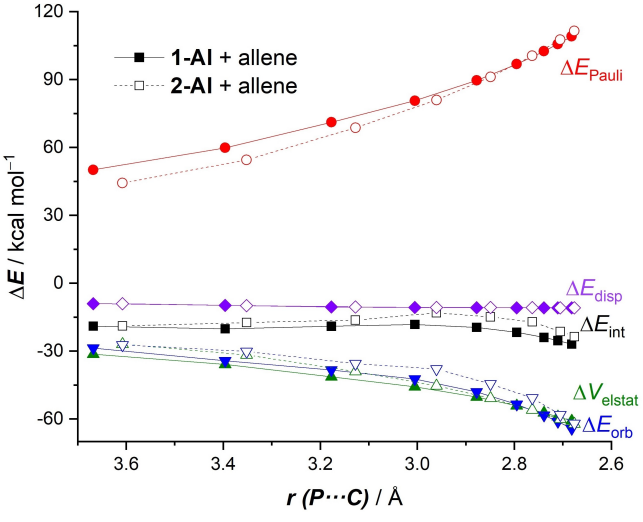

Figure 3. Comparative activation strain analyses of the allene activation reactions mediated by **1-Al** (solid lines) and **2-Al** (dashes lines) projected onto the P···C bond-forming distance. All data have been computed at the ZORA-B3LYP-D3/TZ2P//PCM(benzene)-B3LYP-D3/def2-SVP level.

Journal of Inorganic and General Chemistry
ZAAC
Zeitschrift für anorganische und allgemeine Chemie

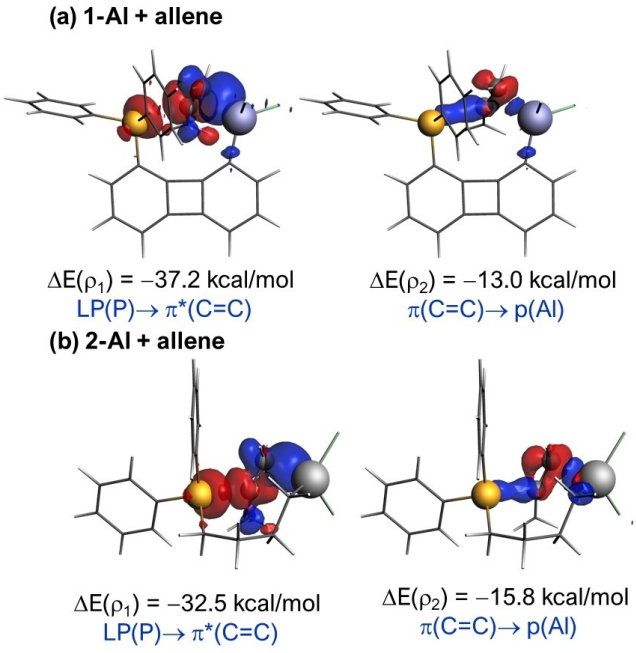

Figure 4. Contour plots of the NOCV deformation densities ϱ and the associated energies ΔE(ϱ)for the main orbital interactions between allene and the intramolecular FLPs **1-Al** (a) and **2-Al** (right). The electronic charge flows from red to blue. All data were computed at the ZORA-B3LYP-D3/TZ2P//PCM(benzene)-B3LYP-D3/def2-SVP level.

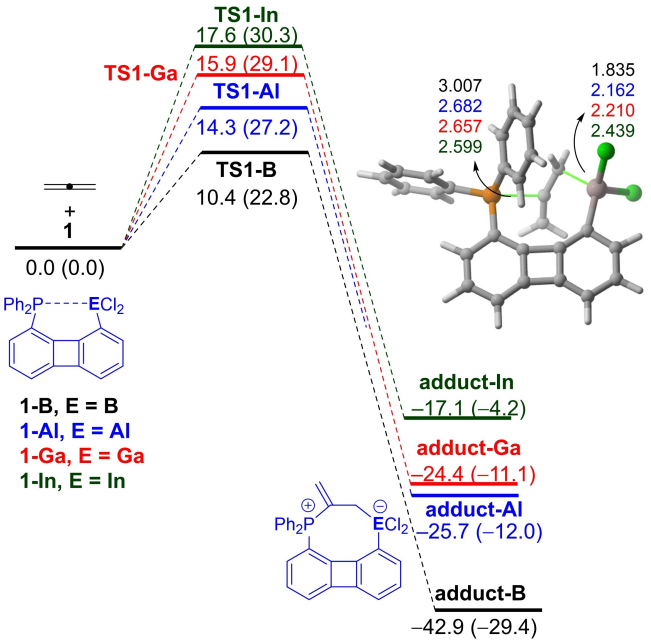

Figure 5. Computed reaction profiles for the allene activations promoted by FLPs **1-E** (E = B to In). Relative electronic (ΔE) and free (ΔG, within parentheses) energies and bond distances are given in kcal/mol and angstroms, respectively. All data have been computed at the PCM(benzene)-M06-2X/def2-TZVPP//PCM(benzene)-B3LYP-D3/def2-SVP level.

confirm the cooperative action of both Lewis antagonists in the activation of allene, which resembles that in related activation reactions of other small molecules.[13,14] Interestingly, the energies associated with these orbital interactions (ΔE(ϱ)), computed at the same consistent P···C bond-forming distance of 2.7 Å,[28] clearly indicate that while the ϱ_2 interaction is rather similar in both processes, the interaction involving the Lewis base (ϱ_1) is significantly stronger for the process involving **1-Al** as compared to **2-Al** ($\Delta\Delta E(\varrho_1) = 4.7$ kcal/mol). This stronger interaction is therefore mainly responsible for the computed stronger orbital interactions which result in a stronger total interaction for the process involving **1-Al**. Therefore, our ASM-EDA(NOCV) approach suggests that the enhanced reactivity of the strained FLP **1-Al** over its counterpart **2-Al**, having a more flexible tether, results from a less destabilizing deformation energy to adopt the corresponding transition state geometry together with a stronger LP(P)→π*(allene) orbital interaction which significantly increases the interaction between the deformed reactants along the entire reaction coordinate.

Once the factors governing the enhanced reactivity of the experimentally described strained FLP **1-Al** have been disclosed, we then explored the influence of the nature of the Lewis acid atom on the reactivity. To this end, we compared the analogous activation reactions of allene promoted by the same strained species having different group 13 elements in their structures.

From the computed reaction profiles in Figure 5, it is confirmed that in all cases the activation reaction occurs in a concerted manner through the corresponding eight-membered transition state. Data in Figure 5 indicate that the reactivity of the system becomes lower and lower when going down in group 13 (B > Al > Ga > In) from both kinetic and thermodynamic points of view. Thus, the transformation proceeds with a higher activation barrier and becomes less exothermic when the group 13 atom goes from B to In. Interestingly, the key P···C bond-forming distance in the corresponding transition states becomes shorter and shorter from **TS1-B** to **TS1-In**, which indicates that the transition states are reached later and later. We can then conclude that late transition states in these FLP-mediated activation reactions are associated with higher activation barriers than earlier transition states, which is fully consistent with the Hammond–Leffer postulate.[29] Indeed, very good linear correlations were found when plotting either the $\Delta E^{\neq}$ or $\Delta G^{\neq}$ values versus the P···C distances in the transition states (see Figure S3 in the Supporting Information).

To understand the reasons behind this reactivity trend, the ASM-EDA(NOCV) approach was then applied. From the ASDs in Figure 6, once again showing the allene activation reactions mediated by **1-E** (E = B to In) from the initial stages of the transformation to the respective transition states and projected onto the P···C bond-forming distance, it becomes clear that the higher barriers computed for the heavier systems **1-Ga** and **1-In** in comparison to **1-Al** result from a much weaker interaction energy between the deformed reactants along the entire reaction coordinate despite these processes benefit from a less destabilizing strain energy. The situation in the most reactive FLP **1-B** is rather particular as this species leads to a much

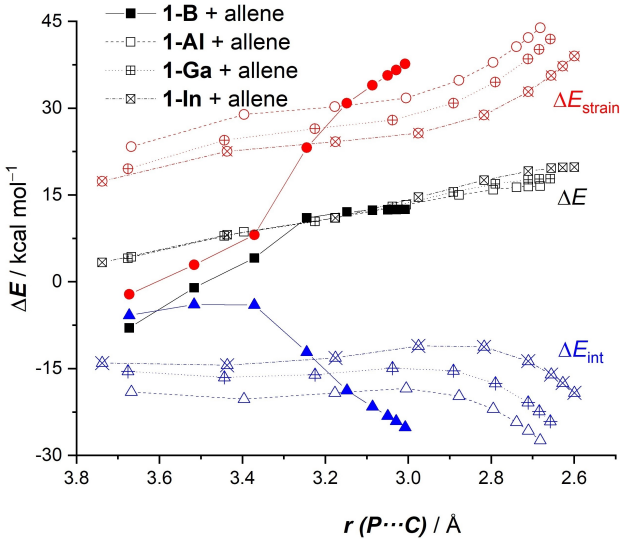

Figure 6. Comparative activation strain analyses of the allene activation reactions mediated by **1-E** (E = B to In) projected onto the P···C bond-forming distance. All data have been computed at the PCM(benzene)-B3LYP-D3/def2-TZVPP//PCM(benzene)-B3LYP-D3/def2-SVP level.

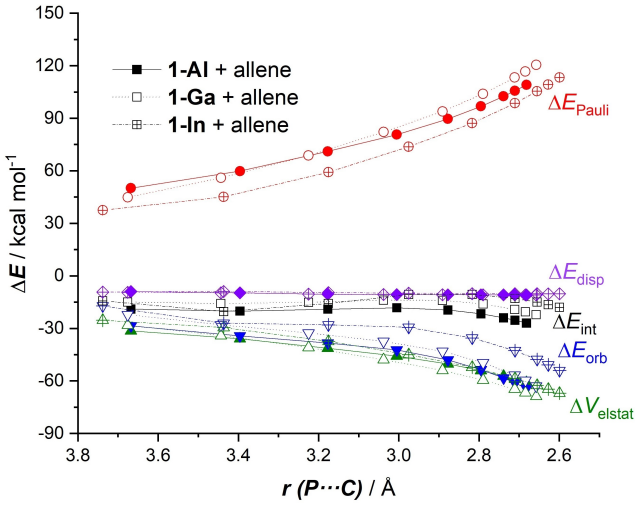

Figure 7. Comparative activation strain analyses of the allene activation reactions mediated by **1-E** (E = Al to In) projected onto the P···C bond-forming distance. All data have been computed at the ZORA-B3LYP-D3/TZ2P//PCM(benzene)-B3LYP-D3/def2-SVP level.

earlier transition state (P···C distance of 3.0 Å) than their heavier counterparts (P···C distance of ca. 2.6 Å). As a consequence, the corresponding ASD suggests that the lower barrier of the process involving **1-B** (in comparison with **1-Al**) derives mainly from a less destabilizing strain energy as the energy penalty to deform the reactants is comparatively much lower.

We finally applied the EDA(NOCV) method to understand the factors leading to the weaker interaction in the processes mediated by the heavier systems **1-Ga** and **1-In** in comparison to that promoted by **1-Al**. As graphically shown in Figure 7, despite the process mediated by **1-Ga** benefits from slightly stronger electrostatic interactions and that promoted by **1-In** from a less destabilizing Pauli repulsion, the trend in ΔE_{int} (Al > Ga > In) is mainly due to the key orbital interactions, which follows the same trend. For instance, as the same consistent P···C bond-forming distance of 2.7 Å, $\Delta E_{orb} = -62.4$ kcal/mol (**1-Al**) > −57.9 kcal/mol (**1-Ga**) > −43.7 kcal/mol (**1-In**). Not surprisingly, this originates, according to the NOCV extension of the EDA method, from the key LP(P)→π*(allene) orbital interaction which becomes weaker and weaker when going from **1-Al** ($\Delta E(\varrho_1) = -37.3$ kcal/mol) to **1-Ga** ($\Delta E(\varrho_1) = -34.4$ kcal/mol) and to **1-In** ($\Delta E(\varrho_1) = -22.2$ kcal/mol).

Conclusions

From the present computational study, it can be concluded that the enhanced reactivity of the strained intramolecular FLP **1-Al**, featuring a rigid biphenylene linker connecting the LA and LB centers, finds its origin in the much lower deformation energy required to adopt the geometry of the corresponding transition state and also in the stronger interaction between the deformed reactants along the entire reaction coordinate. In comparison with an analogous system having a more flexible tether, the lower deformation energy directly results from the already strained geometry of the initial FLP which better fits the geometry of the corresponding transition state. On the other hand, the stronger interaction between the deformed reactants originates almost exclusively from a stronger LP(P)→π*(allene) orbital interaction. Moreover, our calculations indicate that the nature of the Lewis acid strongly influences the reactivity of these strained FLPs. It is found that the reactivity of these species steadily decreases when going down in group 13 (B > Al > Ga > In) from both kinetic and thermodynamic points of view and, interestingly, the processes proceed through later and later transition states.

Acknowledgements

This work was supported by the Spanish MCIN/AEI/10.13039/501100011033 (Grants PID2019-106184GB-I00 and RED2018-102387-T). S. P. acknowledges the MCIN for a FPI grant.

Conflict of Interest

The authors declare no conflict of interest.

Data Availability Statement

The data that support the findings of this study are available in the supplementary material of this article.

Keywords: Frustrated Lewis Pairs · strain · group 13 · reactivity · DFT calculations

[1] G. C. Welch, R. R. San Juan, J. D. Masuda, D. W. Stephan, *Science* **2006**, *314*, 1124–1126.
[2] For leading reviews, see: a) D. W. Stephan, G. Erker, *Angew. Chem. Int. Ed.* **2010**, *49*, 46–76; *Angew. Chem.* **2010**, *122*, 50–81; b) G. Erker, *Pure Appl. Chem.* **2012**, *84*, 2203–2217; c) D. W. Stephan, G. Erker, *Top. Curr. Chem.*, vol. *332*: *Frustrated Lewis Pairs I*, Springer, Heidelberg, **2013**; d) D. W. Stephan, G. Erker, *Chem. Sci.* **2014**, *5*, 2625–2641; e) D. W. Stephan, *J. Am. Chem. Soc.* **2015**, *137*, 10018–10032; f) D. W. Stephan, G. Erker, *Angew. Chem. Int. Ed.* **2015**, *54*, 6400–6441; *Angew. Chem.* **2015**, *127*, 6498–6541; g) D. W. Stephan, *Acc. Chem. Res.* **2015**, *48*, 306–316; h) D. W. Stephan, *Science* **2016**, *354*, aaf7229.
[3] See also: a) A. R. Jupp, D. W. Stephan, *Trends Chem.* **2019**, *1*, 35–48; b) D. W. Stephan, *Chem* **2020**, *6*, 1520–1526.
[4] a) J. Lam, K. M. Szkop, E. Mosaferi, D. W. Stephan, *Chem. Soc. Rev.* **2019**, *48*, 3592–3612; b) W. Meng, X. Feng, H. Du, *Acc. Chem. Res.* **2018**, *51*, 191–201; c) D. W. Stephan, *J. Am. Chem. Soc.* **2021**, *143*, 20002–20014; d) M. G. Guerzoni, A. Dasgupta, E. Richards, R. L. Melen, *Chem Catalysis* **2022**, *11*, 2865–2875.
[5] M. Hong, J. Chen, E. Y. Chen, *Chem. Rev.* **2018**, *118*, 10551–10616.
[6] a) K. K. Ghuman, T. E. Wood, L. B. Hoch, C. A. Mims, G. A. Ozin, C. V. Singh, *Phys. Chem. Chem. Phys.* **2015**, *17*, 14623–14635; b) Z. Niu, W. D. C. Bhagya Gunatilleke, Q. Sun, P. C. Lan, J. Perman, J.-G. Ma, Y. Cheng, B. Aguila, S. Ma, *Chem* **2018**, *4*, 2587–2599.
[7] Selected representative examples: a) C. Appelt, H. Westenberg, F. Bertini, A. W. Ehlers, J. C. Slootweg, K. Lammertsma, W. Uhl, *Angew. Chem. Int. Ed.* **2011**, *50*, 3925–3928; *Angew. Chem.* **2011**, *123*, 4011–4014; b) C. Appelt, J. C. Slootweg, K. Lammertsma, W. Uhl, *Angew. Chem. Int. Ed.* **2012**, *51*, 5911v5914; *Angew. Chem.* **2012**, *124*, 6013–6016; c) L. Keweloh, H. Klöcker, E.-U. Würthwein, W. Uhl, *Angew. Chem. Int. Ed.* **2016**, *55*, 3212–3215; *Angew. Chem.* **2016**, *128*, 3266–3269; d) B. Waerder, M. Pieper, L. A. Körte, T. A. Kinder, A. Mix, B. Neumann, H.-G. Stammler, N. W. Mitzel, *Angew. Chem. Int. Ed.* **2015**, *54*, 13416–13419; *Angew. Chem.* **2015**, *127*, 13614–13617; e) P. Holtkamp, F. Friedrich, E. Stratmann, A. Mix, B. Neumann, H.-G. Stammler, N. W. Mitzel, *Angew. Chem. Int. Ed.* **2019**, *58*, 5114–5118; *Angew. Chem.* **2019**, *131*, 5168–5172; f) L. Wickemeyer, N. Aders, A. Mix, B Neumann, H.-G. Stammler, J. J. Cabrera-Trujillo, I. Fernández, N. W. Mitzel, *Chem. Sci.* **2022**, *13*, 8088–8094.
[8] a) S. Arndt, M. Rudolph, A. S. K. Hashmi, *Gold Bull.* **2017**, *50*, 267v282; b) J. Campos, *J. Am. Chem. Soc.* **2017**, *139*, 2944–2947; c) N. Hidalgo, J. J. Moreno, M. Pérez-Jiménez, C. Maya, J. López-Serrano, J. Campos, *Chem. Eur. J.* **2020**, *26*, 5982–5993.
[9] P. Federmann, T. Bosse, S. Wolff, B. Cula, C. Herwig, C. Limberg, *Chem. Commun.* **2022**, *58*, 13451–13454.
[10] a) I. Fernández, F. M. Bickelhaupt, *Chem. Soc. Rev.* **2014**, *43*, 4953–4967; b) L. P. Wolters, F. M. Bickelhaupt, *WIREs Comput. Mol. Sci.* **2015**, *5*, 324–343; c) F. M. Bickelhaupt, K. N. Houk, *Angew. Chem. Int. Ed.* **2017**, *56*,10070–10086; *Angew. Chem.* **2017**, *129*, 10204–10221. See also d) I. Fernández, in *Discovering the Future of Molecular Sciences* (Ed.: B.Pignataro), Wiley-VCH, Weinheim, **2014**, pp. 165–187.
[11] For reviews on the EDA method, see: a) F. M. Bickelhaupt, E. J. Baerends, in *Reviews in Computational Chemistry*, (Eds. K. B. Lipkowitz, D. B. Boyd), Wiley-VCH: New York, **2000**, Vol. 15, pp. 1–86; b) M. von Hopffgarten, G. Frenking, *WIREs Comput. Mol. Sci.* **2012**, *2*, 43–62; c) I. Fernández, in *Applied Theoretical Organic Chemistry*, (Ed. D. J. Tantillo), World Scientific, New Jersey, **2018**, pp. 191–226.
[12] Selected recent representative examples: a) D. N. Kamber, S. S. Nguyen, F. Liu, J. S. Briggs, H.-W. Shih, R. D. Row, Z. G. Long, K. N. Houk, Y. Liang, J. A. Prescher, *Chem. Sci.* **2019**, *10*, 9109–9114; b) A. Couce-Ríos, A. Lledós, I. Fernández, G. Ujaque, *ACS Catal.* **2019**, *9*, 848–858S; c) I. Fernández, *Chem. Sci.* **2020**, *11*, 3769–3779; d) P. Vermeeren, T. A. Hamlin, I. Fernández, F. M. Bickelhaupt, *Angew. Chem. Int. Ed.* **2020**, *59*, 6201–6206; *Angew. Chem.* **2020**, *132*, 6260–6265; e) P. Vermeeren, T. A. Hamlin, I. Fernández, F. M. Bickelhaupt, *Chem. Sci.* **2020**, *11*, 8105–8112; f) T. A. Hamlin, F. M. Bickelhaupt, I. Fernández, *Acc. Chem. Res.* **2021**, *54*, 1972–1981; g) T. Hansen, P. Vermeeren, F. M. Bickelhaupt, T. A. Hamlin, *Angew. Chem. Int. Ed.* **2021**, *60*, 20840–20848; *Angew. Chem.* **2021**, *133*, 21008–21016.
[13] a) D. Yepes, P. Jaque, I. Fernández, *Chem. Eur. J.* **2016**, *22*, 18801–18809; b) D. Yepes, P. Jaque, I. Fernández, *Chem. Eur. J.* **2018**, *24*, 8833–8840; c) J. J. Cabrera-Trujillo, I. Fernández, *Chem. Eur. J.* **2018**, *24*, 17823–17831; d) J. J. Cabrera-Trujillo, I. Fernández, *J. Phys. Chem. A* **2019**, *123*, 10095–10101; e) J. J. Cabrera-Trujillo, I. Fernández, *Inorg. Chem.* **2019**, *58*, 7828–7836; f) J. J. Cabrera-Trujillo, I. Fernández, *Chem. Eur. J.* **2021**, *27*, 3823–3831; g) J. J. Cabrera-Trujillo, I. Fernández, *Chem. Commun.* **2022**, *58*, 6801–6804. For a recent EDA study in transition-metal based FLPs, see: h) E. A. Ison, J. L. Tubb, *Inorg. Chem.* **2021**, *60*, 13797–13805.
[14] For a Feature article, see: I. Fernández, *Chem. Commun.* **2022**, *58*, 4931–4940.
[15] Gaussian 09, Revision D.01, M. J. Frisch, G. W. Trucks, H. B. Schlegel, G. E. Scuseria, M. A. Robb, J. R. Cheeseman, G. Scalmani, V. Barone, G. A. Petersson, H. Nakatsuji, X. Li, M. Caricato, A. Marenich, J. Bloino, B. G. Janesko, R. Gomperts, B. Mennucci, H. P. Hratchian, J. V. Ortiz, A. F. Izmaylov, J. L. Sonnenberg, D. Williams-Young, F. Ding, F. Lipparini, F. Egidi, J. Goings, B. Peng, A. Petrone, T. Henderson, D. Ranasinghe, V. G. Zakrzewski, J. Gao, N. Rega, G. Zheng, W. Liang, M. Hada, M. Ehara, K. Toyota, R. Fukuda, J. Hasegawa, M. Ishida, T. Nakajima, Y. Honda, O. Kitao, H. Nakai, T. Vreven, K. Throssell, J. A. Montgomery, Jr., J. E. Peralta, F. Ogliaro, M. Bearpark, J. J. Heyd, E. Brothers, K. N. Kudin, V. N. Staroverov, T. Keith, R. Kobayashi, J. Normand, K. Raghavachari, A. Rendell, J. C. Burant, S. S. Iyengar, J. Tomasi, M. Cossi, J. M. Millam, M. Klene, C. Adamo, R. Cammi, J. W. Ochterski, R. L. Martin, K. Morokuma, O. Farkas, J. B. Foresman, D. J. Fox, Gaussian, Inc., Wallingford CT, **2016**.
[16] a) A. D. Becke, *J. Chem. Phys.* **1993**, *98*, 5648–5652; b) C. Lee, W. Yang, R. G. Parr, *Phys. Rev. B* **1998**, *37*, 785–789; c) S. H. Vosko, L. Wilk, M. Nusair, *Can. J. Phys.* **1980**, *58*, 1200–1211.
[17] S. Grimme, J. Antony, S. Ehrlich, H. Krieg, *J. Chem. Phys.* **2010**, *132*, 154104–19.
[18] F. Weigend, R. Ahlrichs, *Phys. Chem. Chem. Phys.* **2005**, *7*, 3297–3305.
[19] a) S. Miertuš, E. Scrocco, J. Tomasi, *Chem. Phys.* **1981**, *55*, 117–129; b) J. L. Pascual-Ahuir, E. Silla, I. Tuñón, *J. Comput. Chem.* **1994**, *15*, 1127–1138; c) V. Barone, M. Cossi, *J. Phys. Chem. A* **1998**, *102*, 1995–2001.
[20] C. Gonzalez, H. B. Schlegel, *J. Phys. Chem.* **1990**, *94*, 5523–5527.
[21] Y. Zhao, D. G. Truhlar, *Theor. Chem. Acc.* **2008**, *120*, 215–241.
[22] M. P. Mitoraj, A. Michalak, T. Ziegler, *J. Chem. Theory Comput.* **2009**, *5*, 962–975.
[23] a) G. Te Velde, F. M. Bickelhaupt, E. J. Baerends, C. Fonseca Guerra, S. J. A. Van Gisbergen, J. G. Snijders, T. Ziegler, *J. Comput. Chem.* **2001**, *22*, 931–967; b) *ADF2020*, SCM, Theoretical Chemistry, Vrije Universiteit, Amsterdam, The Netherlands, http://www.scm.com.
[24] J. G. Snijders, P. Vernooijs, E. J. Baerends, *At. Data Nucl. Data Tables* **1981**, *26*, 483–574.

[25] J. Krijn, E. J. Baerends, *Fit Functions in the HFS-Method*, Internal Report (in Dutch), Vrije Universiteit Amsterdam, The Netherlands, **1984**.
[26] a) E. van Lenthe, E. J. Baerends, J. G. Snijders, *J. Chem. Phys.* **1993**, *99*, 4597–4610; b) E. van Lenthe, E. J. Baerends, J. G. Snijders, *J. Chem. Phys.* **1994**, *101*, 9783–9792; c) E. van Lenthe, A. Ehlers, E. J. Baerends, *J. Chem. Phys.* **1999**, *110*, 8943–8953.
[27] a) T. A. Hamlin, B. J. Levandowski, A. K. Narsaria, K. N. Houk, F. M. Bickelhaupt, *Chem. Eur. J.* **2019**, *25*, 6342–6348; b) Y. García-Rodeja, I. Fernández, *J. Org. Chem.* **2019**, *84*, 4330–4337.
[28] Performing this analysis at a consistent point along the reaction coordinate (near all transition structures), rather than the transition state alone, ensures that the results are not skewed by the position of the transition state.
[29] a) J. E. Leffler, *Science* **1953**, *117*, 340–341; b) G. S. A. Hammond, J . *Am. Chem.* **1955**, *77*, 334–338.

Manuscript received: December 19, 2022
Revised manuscript received: January 12, 2023
Accepted manuscript online: January 12, 2023

